Polypropylene cracking on embryonic and ZSM-5 catalysts – An *operando* study

Karolina A. Tarach [a], Mariame Akouche [b], Kamila Pyra [a], Valentin Valtchev [b], Gabriela Jajko [a,c], Jean-Pierre Gilson [b], Kinga Góra-Marek [a,*]

[a] *Faculty of Chemistry, Jagiellonian University in Krakow, Gronostajowa 2, 30-387 Krakow, Poland*
[b] *Normandie Université, ENSICAEN, UNICAEN, CNRS, Laboratoire Catalyse & Spectrochimie, 14000 Caen, France*
[c] *Doctoral School of Exact and Natural Sciences, Jagiellonian University in Krakow, Łojasiewicza 11, 30-348 Krakow, Poland*

ARTICLE INFO

ABSTRACT

A series of ZSM-5 zeolites (embryonic, microporous, hierarchical) is studied in the catalytic cracking of polypropylene in the framework of its chemical recycling. Two important zeolite features impact their catalytic performances and allow their design as efficient catalysts: porosity and acidity. They also play a key role in catalyst deactivation and regeneration. A detailed thermogravimetric and spectroscopic (*operando* FT-IR) analysis of the reaction, including catalyst coking and regeneration, shows the emergence of rules to design fit-for-purpose catalysts to be used in existing or grass-roots FCC units.

1. Introduction

A wide variety of plastics meet the requirements of many segments of the economy in a cost-competitive way. Polypropylene (PP) and polyethylene (PE) are the most common type of polyolefins, and their 2022 market size is nearly USD 300 billion with a predicted 5% CAGR (Compound Annual Growth Rate) till 2030 [1]; they account for more than 2/3 of the annual plastics production. One application, consumer product packaging, is in direct daily contact with people, *i.e.*, each of us. A so far inefficient collection of these and all non-biodegradable plastics generates an unsustainable amount of severe pollution, marine plastics being the highly visible tip of this iceberg. Currently, only 16% of plastic waste is reused to make new plastics, with less than 1% chemically reprocessed to provide the original building blocks, *i.e.*, a true circular economy. So, a large proportion of plastics is either left scattered in nature, landfilled, mechanically (down)recycled, or incinerated [1]. Depolymerization back to the original monomers is ideally the best approach to chemical recycling and is already taking place for some polyamides and polyesters. It is not yet the case for polyolefins, although they contribute significantly to plastic waste. Their thermal cracking produces a broad range of hydrocarbons requiring further processing to meet the requirements of transportation fuels or higher value (petro) chemicals [2]. Catalysis has a role to play in solving such an important societal challenge. Catalytic cracking, for instance, could bring a

combination of higher activity and better selectivity control (narrower product distribution requiring less downstream processing) while working under milder operating conditions (*e.g.*, temperature). All these features indicate potential economic benefits; moreover, catalytic solutions could benefit from the vast experience of existing processes (*e.g.*, FCC [Fluid Catalytic Cracking]), practiced and optimized over at least 70 years on a large scale. Catalytic cracking of polyolefins (polyethylene PE, polypropylene PP) to produce their olefinic monomers has already received attention in previous studies using zeolites [3]. They deserve special attention as their acid sites located in well-defined micropores (~ 0.5–1.0 nm) contribute greatly to the upgrading of heavy oil fractions (atmospheric and vacuum residues) to gasoline ($C_{5–11}$) and/or lower olefins ($C_{3–5}$) [4]. Polyolefins are intrinsically a less complex feedstock than heavy oil fractions as they are made mostly of C-C and C-H bonds. The heavy oil fractions contain significant amounts of S, N, metals (Fe, Ni, V…) spread between many high molecular weight hydrocarbons with high C/H ratios (*e.g.*, polyaromatics) poisoning many catalysts. The downside of zeolites is the presence of severe diffusion limitations resulting in limited use of all their potential "active" sites when bulky molecules are involved. One of the earliest explored remedies is the design of hierarchical zeolites where connected mesopores are added post-synthesis to the pristine micropores, a so-called top-down route. An alternative bottom-up strategy is to synthesize small zeolite crystals, the so-called nano-zeolites [5]. Another promising approach could be based

---

* Corresponding author.
E-mail address: kinga.gora-marek@uj.edu.pl (K. Góra-Marek).

on the so-called embryonic zeolites (EZ) [6,7]; these X-ray amorphous materials, harvested in the early stages of zeolite synthesis, lack the long-range order of zeolites, but their active sites are more accessible enabling the conversion of bulky molecules such as 1,3,5 – triisopropylbenzene (TiPBz, kinetic diameter: 1.1 nm) as their pore size can be engineered in a wider range (1 −2.5 nm) [8]. While TiPBz can also be dealkylated on μm-sized ZSM-5, this can only occur on the very few acid sites present on the external surface of the crystals. EZ also possess an advantage over amorphous Silica-Aluminas (ASA) as their tetrahedral Al is more resilient to thermal treatments and therefore keep more of their original acidity due to a reduced dealumination. EZ could therefore extend the range of applications of current zeolites in the processing of polyolefins [9].

The present work investigates for the first time the potential use of these acidic X-ray amorphous EZ to deconstruct polypropylene into useful lower molecular weight molecules. They are compared to a purely microporous ZSM-5 and hierarchical zeolites produced by caustic leaching biased towards desilication [8]. Particular attention is paid to the effect of acid site strength (related to the confined environment) and pore dimensions.

2. Experimental

2.1. Materials

2.1.1. EZ-ZSM-5 and H-ZSM-5

The embryonic zeolite was prepared according to the procedure described in ref. [7], using a gel with a Si:Al ratio of 50 and tetrapropylammonium (TPA) as a structure-directing agent. This embryonic zeolite is hereinafter referred to as EZ-ZSM-5. The fully crystalline counterpart of EZ, herein denoted as H-ZSM-5, was obtained from the same initial system after crystallization at 150 °C for 2 days.

2.1.2. Hierarchical zeolites

Two hierarchical zeolites are derived from a common ZSM-5 (CBV 28014, SiAl = 150, Zeolyst International) by leaching it with 0.2 M and 0.5 M NaOH solutions at 65 °C for half an hour [10]. Typically, 100 mL of the alkaline solutions are added to 3.0 g of zeolite. After each treatment, the suspension is cooled in an ice-bath and filtered. The resulting hierarchical zeolites are washed with deionized water until neutral pH, ion-exchanged four times with a 0.5 M NH_4NO_3 solution at 60 °C for 1 h then filtered, washed, and dried at room temperature. The two resulting materials are referred to as deSi-0.2-ZSM-5 and deSi-0.5-ZSM-5, where x in deSi-x-ZSM-5 indicates the NaOH concentration in solution; deSi reminds us that during such an hierarchization, Si is preferentially extracted from the zeolite framework.

2.2. Characterization

The chemical composition of the catalysts is determined by inductively coupled plasma optical emission spectrometry (ICP-OES, Optima 2100DV, PerkinElmer).

The powder X-ray diffractions are recorded on a Rigaku Multiflex diffractometer using the Cu Kα radiation (40 kV, 40 mA).

Transmission Electron Microscopy (TEM) of the materials is done on a JEOL-2011 F with an acceleration voltage of 200 kV. Prior to characterization, all samples are dispersed in isopropanol and ultrasonicated for 30 min and then dropped onto a carbon film on a copper grid.

The porosity is measured by nitrogen adsorption/desorption isotherms on a Quantachrome Autosorb− 1-MP volumetric analyser. All samples are degassed under 10^{-5} mbar at 350 oC for 24 h before measurement. The specific surface area, S_{BET}, is calculated using the Brunauer-Emmett-Teller method, and the total pore volume (V_{total}) is taken from the nitrogen volume adsorbed at $p/p_0 = 0.985$. The micropore volume (V_{micro}) is calculated using the t-plot method and the mesopore volume (V_{meso}) is BJH adsorption cumulative volume of pores

between 1.7 and 30 nm diameter. By anology, the S_{meso} is BJH adsorption cumulative surface area.

The acidic features of the catalysts are assessed by IR monitoring of adsorbed probes (CO and Pyridine). All IR spectra are recorded with a resolution of 2 cm^{-1} on a Bruker Invenio X FT-IR spectrometer fitted with an MCT detector in the range 4000–400 cm^{-1}. The samples are pressed into self-supported wafers (10 mg per 1 cm^2), placed in an IR cell connected to a vacuum line, activated under vacuum (10^{-6} torr) at 500 °C for 1 h and then cooled down to acquire the spectra at room temperature.

CO (Linde Gas Poland, 99.95%) is adsorbed at − 140 °C up to saturation of the Lewis acidic sites (bands at 2230, 2225 cm^{-1} and 2190 cm^{-1}) and the appearance of hydrogen-bonded CO to Brønsted Si(OH)Al sites (band at 2175 cm^{-1}).

Pyridine (Py) (Avantor) is adsorbed at 170 °C. Each sample is saturated with Py and the cell evacuated at 170 °C to remove gaseous and physisorbed Py. The Brønsted (BAS) and Lewis (LAS) acid sites concentration are obtained from the integrated area of the adsorbed pyridine bands at 1560 − 1535 (pyridinium ions, PyH^+) and 1440 − 1460 cm^{-1} (Py-Lewis site adduct) by using extinction coefficients reported earlier [11]. The acid strength is assessed by Py thermodesorption, where all samples are heated to 350 °C, kept there for 10 min, cooled to 170 °C where IR spectra are recorded. The ratio between Py adsorbed at 350 °C and 170 °C describes the acid strength of the various catalysts.

The Brønsted acid sites located on the external and mesoporous surfaces of ZSM-5 are quantified by IR monitoring of the adsorption at 200 °C of 2,6-di-tert-butylpyridine (di-TBPy, Sigma–Aldrich, >97%, kinetic diameter: 0.8 nm), desorption under vacuum at 200 °C (15 min) and cooling down to room temperature. The 1615 cm^{-1} band intensities of di-TBPyH$^+$ (molar extension coefficient 0.50 $cm^2 \cdot \mu mol^{-1}$) are used to quantify the number of di-TBPy-accessible acid sites [12]. The intensity of di-TBPyH$^+$ band is calculated from the spectra recorded after di-TBPy adsorption at 200 °C for 15 min, subsequently cooled down to room temperature. All spectra are normalized to a 10 mg weight of sample.

2.3. Catalytic cracking of polypropylene

Low density polypropylene, PP, (Alfa Aesar, Product No.: 42607, Lot No.: P28D047) is crushed, sieved and the ≤ 250 μm fraction retained for testing. The catalytic cracking of PP takes place in a thermobalance (TGA/SDTA Mettler Toledo). 10 mg of zeolite powder is mixed for 10 min with PP (30 mg) in an agate mortar, 10 mg are transferred to an α-Al$_2$O$_3$ crucible in the thermobalance. The polymer cracking takes place within the 30–600 °C temperature range under a heating rate of 5 °C/min under N_2 flow (80 mL·min^{-1}). The catalyst weight and adsorbed moisture are considered to calculate the degree of conversion and level of coke left on the catalysts. After the reaction, all samples are cooled to 30 °C and then flushed with dry synthetic air (80 mL·min^{-1}). The coke content is the mass change after heating to 800 °C at a rate 30 °C·min^{-1}. For comparative purposes, pure PP is cracked thermally, i. e., without any catalyst. The TGA is connected with GC-MS setup to follow the evolved products.

2.4. FT-IR and GC&MS operando

An *operando* setup is used to study the PP degradation. A self-supporting disc (*ca.* 5.5–6 mg·cm^{-2}) of the catalyst and PP in 1:1 ratio is placed in a 2 cm^3-volume quartz IR cell (MeasLine, www.measline. com, patent PL232633, Poland). The homogeneity of the zeolite/catalyst mixtures is identical to the TGA setup and the room temperature IR spectra are normalized to the same intensity of the overtone bands (2050 −1800 cm^{-1}). As in each spectrum, the intensity of the 2960 cm^{-1} (–CH$_3$) and 2925 cm^{-1} (–CH$_2$) bands are similar, an equal amount of catalyst can be assumed. During the reaction, the catalyst surface as well as the gas phase are monitored simultaneously, Fig. 1. N$_2$, the carrier gas (flow rate = 30 mL/min, 110 °C) is introduced along Teflon lines (1/
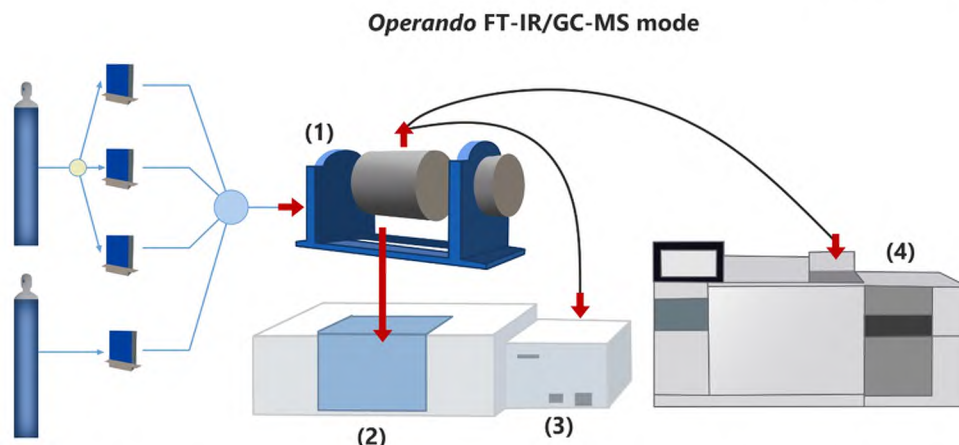
Fig. 1. Operando IR cell fed by independently controlled flowing gases (1), coupled to four detectors: IR spectrometer (2), IR gas cell (3), GC-MS (4).

16'') and the *operando* IR cell with the catalyst/PP wafer heated from room temperature to 250 °C (ramp of 10 °C·s^{-1}) till full polymer conversion. Time-resolved spectra are collected on the FT-IR spectrometer and the products simultaneously analysed by mass spectrometry (MeasLine, www.measline.com, RGA200) and gas chromatography (Agilent Technologies 7890B). Coke and tars are included to compute catalyst selectivity.

2.5. 2D COS analysis of FT-IR spectroscopy results

Due to the complexity of polymer cracking, a two-dimensional correlation analysis (2D COS IR) is helpful to monitor both the PP cracking and the subsequent coke combustion on a catalytically active surface. 2D maps with contour plots along two axes (wavenumbers and correlation intensity) enable better monitoring of the reaction as a function of time on stream than conventional 1D spectra with numerous overlapping bands. Typically, a synchronous 2D correlation map highlights simultaneous or coincident events identified by two separate bands (ν_1 and ν_2) upon an externally triggered perturbation, a chemical reaction in this case. A positive ν_1-ν_2 correlation indicates a simultaneous increase or decrease in the intensity of these bands, while a negative correlation indicates that the intensity of one band (*e.g.*, ν_1) changes at the expense of the other (*e.g.*, ν_2).

3. Results and discussion

3.1. Characterization of the catalysts: structure, texture and acidity

The catalysts used in PP cracking possess similar or different structural, textural, and acidic properties to better assign their performances to specific features. Fig. 2A highlights that EZ-ZSM-5 with a bulk Si/Al ratio of 50 is X-ray amorphous while the purely microporous H-ZSM-5 and hierarchical samples (deSi-0.2-ZSM-5 and deSi-0.5-ZSM-5) all display the MFI-type structure. The deSi-0.5-ZSM-5 hierarchical zeolite and EZ-ZSM-5 have close Si/Al while deSi-0.2-ZSM-5 is less desilicated. The H-ZSM-5 exhibits a type I N_2 adsorption isotherm with a steep nitrogen uptake at low relative pressure, indicating the presence of micropores ($< \sim$1 nm) (Fig. 2B). Textural mesopores are evidenced by a second uptake at higher relative pressures. EZ-ZSM-5 displays a type I(b) N_2 adsorption isotherm characteristic of larger micropores and/or smaller mesopores ($< \sim$ 2.5 nm) [13]. The micropores in H-ZSM-5 and hierarchical zeolites are, as expected, in the 0.50–0.60 nm range. EZ-ZSM-5 has supermicropores ($>$ 0.7 nm), as well as ultra-microporosity (Fig. 2C). The two hierarchical catalysts, deSi-0.5-ZSM-5 and deSi-0.2-ZSM-5, display type IV isotherms with mixed H2 and H4 hysteresis loops [14] in the P/P° range 0.5–0.9 indicative of intracrystalline bottlenecked mesopores and mesopores

connected to the outer surface. Mesoporosity is more important in the two deSi-x-ZSM-5 and centered around 18 nm (Fig. 2D). No mesoporous characteristic is visible on EZ-ZSM-5. The indexed hierarchy factor (IHF, see Table 1) is helpful as it measures the alteration of textural properties [10], *i.e.* higher IHF indicates a greater share of mesopores while microporosity is preserved and lower IHF witness either an excess in microporosity or mesoporosity. In our case, a high hierarchization degree with preserved microporosity occurs only both deSi-0.5-ZSM-5 and EZ-ZSM-5.

TEM micrographs are gathered in Fig. 3. H-ZSM-5 consists of 400 nm aggregates, while EZ-ZSM-5 shows *ca.* 3–8 nm featureless aggregates. The mildly desilicated deSi-0.2-ZSM-5 shows uniform mesopores from the external surface to the interior of the zeolite microporosity. The more severely leached deSi-0.5-ZSM-5 consists of core–shell particles with macropores on its external shell and zeolite mesoporosity elsewhere. The presence of Al-rich external layer can be anticipated form dense shell displayed in deSi-0.5-ZSM-5. These features are consistent with N_2 physisorption indicating the presence of macro- and mesoporosity in deSi-0.5-ZSM-5.

Fig. 4A shows the IR spectra of silanols and bridged hydroxyls on all catalysts. EZ-ZSM-5 stands out with the highest population of isolated $(SiO)_3$Si-OH (3756 cm^{-1}) and internal (3715 cm^{-1}) silanols together with many hydrogen-bonded silanols (broad band around 3510 cm^{-1}). As expected, the silanol population in two desilicated zeolites is high and the increased intensity of isolated Si-OH follows the increasing mesoporous area of deSi-0.5-ZSM-5 and deSi-0.2-ZSM-5 [15]. The bridging hydroxyls, Si(OH)Al, located between 3615 and 3605 cm^{-1} on the three crystalline zeolites are absent on EZ-ZSM-5, a common feature on amorphous aluminosilicates where a wider spread of T-O-T angle leads to negligible intensities of the corresponding Si(OH)Al bands [16]. A more precise analysis of the surface acidity is worth exploring as silanols can sometimes display acidity in the range of bridged hydroxyls and therefore promote hydrocarbon transformation as cracking and coking [17].

Acid site concentration and strength is measured by FT-IR monitoring of Py adsorption (Table 2). The EZ-ZSM-5 and highly mesoporous deSi-0.5-ZSM-5 possess the highest number of LAS, namely 43–50% of the total acidity. The origin of this important Lewis acidity on the embryonic and hierarchical zeolites is further examined by CO adsorption monitored by FT-IR (Fig. 4B). The CO spectra on EZ-ZSM-5 shows a band at 2190 cm^{-1} indicative of its interaction with minor fraction of LAS of weak and/or moderate strength, *i.e.*, extra-framework aluminum species (EFAL species). We showed earlier that after calcination (refs 6,7), only a minor quantity of Al is octahedrally coordinated, in contrast to what happens to conventional ASA's (amorphous silica alumina's) [18]. On deSi-0.5-ZSM-5, bands at 2225–2220 cm^{-1} witness the presence of coordinatively unsaturated of alumina clusters (EFAL species, LAS) with
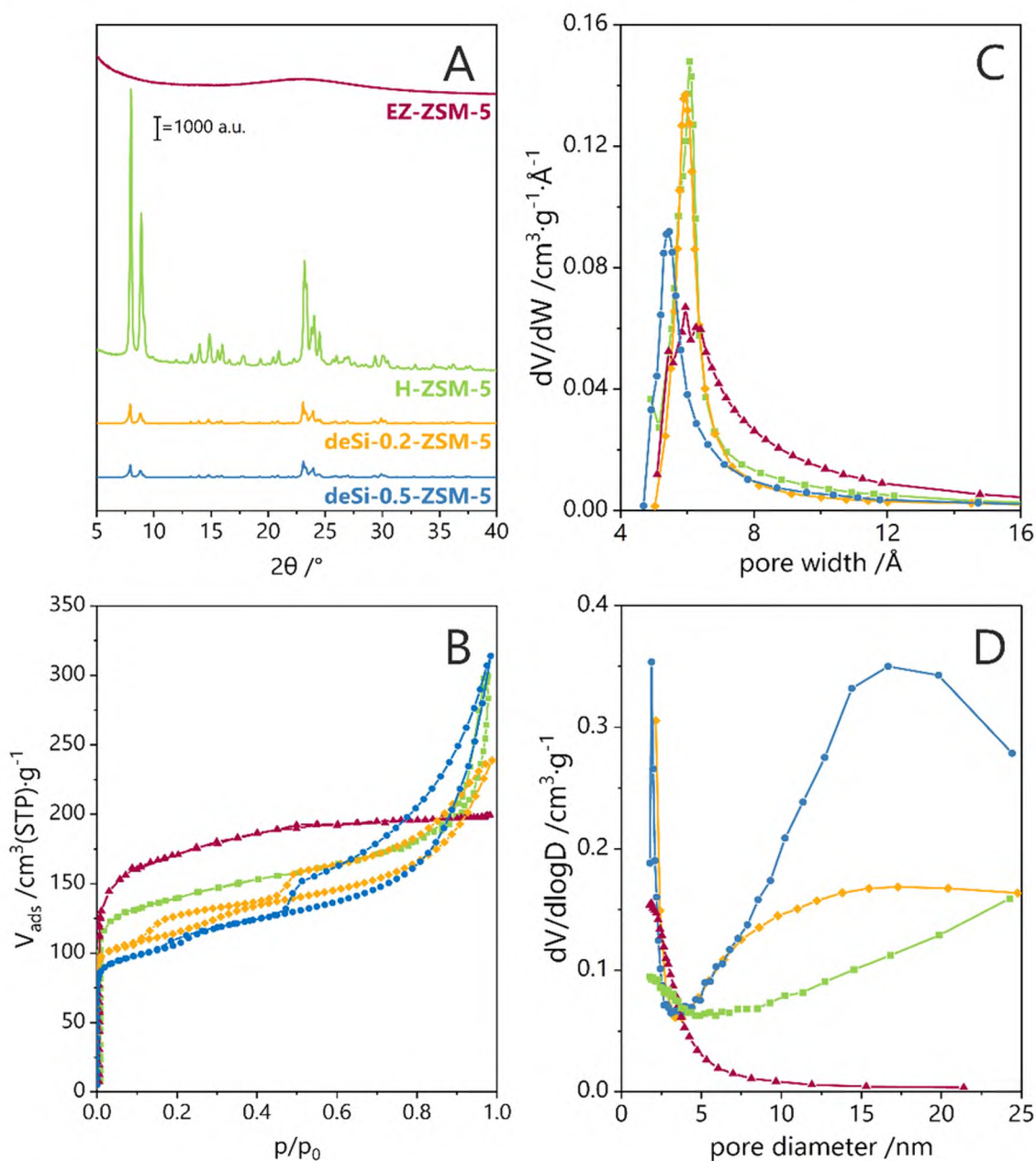
Fig. 2. A) XRD powder patterns. B) N_2 adsorption–desorption isotherms. C) Micropore size distributions. D) BJH pore size distributions.

Table 1
Chemical composition (ICP) and textural properties (N_2 physisorption) data.

Sample	Si/Al^a	$V_{total}\ cm^3g^{-1}$	$V_{micro}^b\ cm^3g^{-1}$	$V_{meso}^c\ cm^3g^{-1}$	$S_{BET}\ m^2g^{-1}$	$S_{micro}\ m^2g^{-1}$	$S_{meso}\ m^2g^{-1}$	IHF^d
EZ-ZSM-5	50	0.30	0.26	0.05	601	575	78	0.34
H-ZSM-5	65	0.62	0.19	0.11	535	447	78	0.25
deSi-0.2-ZSM-5	124	0.40	0.15	0.15	433	335	98	0.25
deSi-0.5-ZSM-5	48	0.49	0.13	0.34	393	278	156	0.36

[a] ICP.

[b] t-plot method with thickness between 4 and 9.2 Å, P/P° (0.05, 0.8).

[c] DFT.

[d] IHF (index hierarchy factor) calculated as $(V_{micro}/V_{micro,max}) \times (S_{meso}/S_{meso,max})$ [10].

high strength formed after dehydroxylation of two neighboring Si(OH) Al species [19,20]. On H-ZSM-5 and deSi-0.2-ZSM-5, both with lower mesoporosity, Brønsted acidity is prevalent as the relative share of LAS does not exceed 25% (Table 2); they could affect accessibility to the microporous acidity. 2,6-di-tert-butylpyridine (di-TBPy) adsorption monitored by FT-IR, widely used to measure the Brønsted acidity of the external/mesoporous surface of zeolites [12,21] is reported in Table 2 with the Accessibility Factor (AF_{BAS} = percentage of BAS concentration measured by di-TBPy *vs.* Py adsorption). As expected, on H-ZSM-5 very few BAS are located on its external surface (AF_{BAS} = 3%) while on
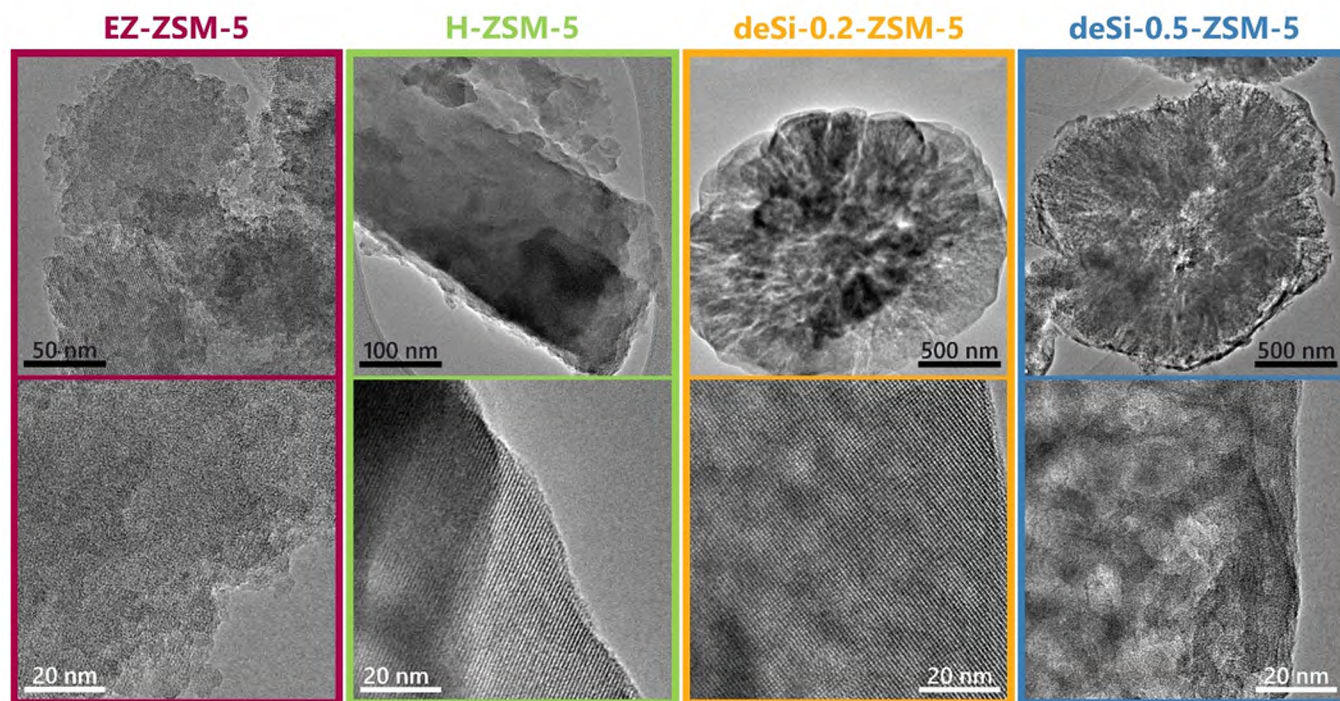
Fig. 3. Transmission electron microscopy images.
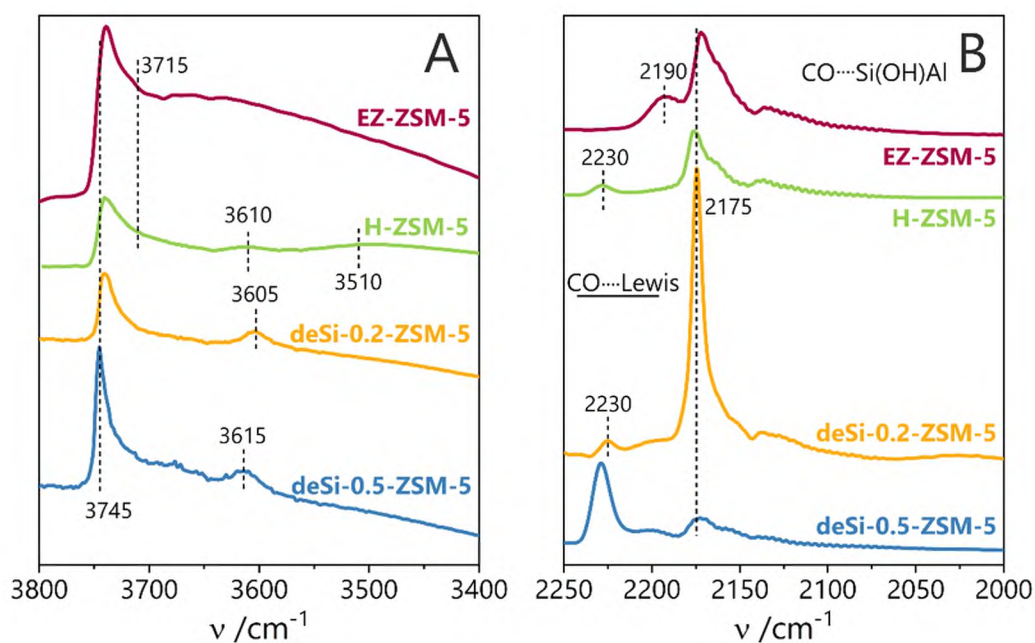
Fig. 4. IR spectra: (A) pristine O-H groups (25 °C) and (B) CO adsorbed on acid sites (−100 °C).

Table 2
Acidity parameters of the catalysts.

Sample	Si/Al	C_{BAS}[a] $\mu mol\ g^{-1}$	C_{LAS}[a] $\mu mol\ g^{-1}$	$C_{BAS} + C_{LAS}$[a] $\mu mol\ g^{-1}$	AF_{BAS}[b] %	ν_{OH}[c] cm^{-1}	BAS[d] A_{350}/A_{170}	LAS[d] A_{350}/A_{170}
EZ-ZSM-5	50	40	30	70	69	–	0.25	0.30
H-ZSM-5	65	115	25	140	3	3610	0.42	0.80
deSi-0.2-ZSM-5	124	95	32	127	50	3605	0.61	0.65
deSi-0.5-ZSM-5	48	140	140	280	33	3615	0.15	0.75

[a] Brønsted (C_{BAS}) and Lewis (C_{LAS}) sites concentration determined by FT-IR (Py adsorption).
[b] Brønsted acid sites accessibility factor (AF_{BAS}), *i.e.*, % of acid sites accessible to di-TBPy *vs.* C_{BAS} accessible to Py.
[c] Strength of the acidic Si(OH)Al measured by the band shift upon hydrogen bonding with CO at − 100 °C (spectra not shown).
[d] Brønsted and Lewis sites strength (A_{350}/A_{170}) determined by FT-IR (Py adsorption).

deSi-0.2-ZSM-5 (high intracrystalline mesoporosity) and EZ-ZSM-5 (high intercrystalline mesoporosity) at least half of the BAS protonate di-TBPy (AF_{BAS} = 50–69%). DeSi-0.5-ZSM-5, with the highest IHF (Table 1) has the lowest AF_{BAS} of the 3 mesoporous catalysts. Realumination followed by dehydroxylation is the most common explanation of the alteration of acid sites in alkaline leached zeolites [10,19]. The high concentration of LAS on deSi-0.5-ZSM-5 is responsible for micropores clogging and limited accessibility of its BAS.

Acid strength is another parameter to consider in zeolitic catalysts. Pyridine thermal desorption, TPD, (A_{350}/A_{170}, Table 2) indicates a potentially higher acid strength of the BAS in H-ZSM-5. The introduction of mesoporosity in ZSM-5 zeolites reduces the apparent acid strength of protonic sites; they appear "weaker" due to differences in confinement between meso- and micropores [22]. The strength of protonic site can also be influenced by close proximity with extraframework Al and silanols [9,23]. The defect-rich EZ-ZSM-5 follows this rule as a lower protonic acid strength appears. The desilicated zeolites can be also considered less perfect with partially extracted Al near framework atoms. It is the case of deSi-0.5-ZSM-5 with a BAS strength similar to EZ-ZSM-5 while deSi-0.2-ZSM-5 possesses the highest protonic strength due to its higher Si/Al as often reported [24,25]. These trends are also aligned with the stretching frequencies of the Si(OH)Al (ν_{OH}, Table 2, Fig. 4A), *i.e.*, the lower ν_{OH}, the longer O-H bond, thus higher the acidity of the corresponding proton. As usual, TPD of basic molecules on hierarchical zeolites should be taken with some caution as differences in diffusion pathlengths could affect diffusion/adsorption ratios of the probe and therefore the maximum temperature in the TPD profile of the basic probe [26].

3.2. Polypropylene cracking: thermogravimetry and operando FT-IR-GC-MS

The effects of the different textural and acidic properties of the above "ZSM-5 catalysts" are tested in the catalytic cracking of PP (polypropylene). Fig. 5A highlights PP conversion (weight loss measured in a thermobalance) as a function of temperature in a typical "light-off" diagram, along with the thermal cracking of pure PP as a reference. T_{10} and T_{80} (temperature for 10% and 80% conversion, Fig. 5D) are used as descriptors. The selectivities of the catalysts are measured in an *operando* FT-IR cell fitted with a GC-MS detector (Fig. 5B).

In the low-temperature range, EZ-ZSM-5 is the most active catalyst, although it has the lowest concentration of acid sites highlighting their higher accessibility coupled with a faster diffusion of reactants and products. Moreover, it cannot be excluded that a portion of the non-bridging silanols could participate in the reaction as their acidity may not be negligible [27]. Indeed, internal H-bonded silanols were already found to be more active and selective compared to external silanols in the Beckmann rearrangement [28]. The EZ sample exhibits the most intense bands at the region typical of hydrogen bonded silanols (3670 – 3100 cm^{-1}), the involvement of the medium and high acidity silanols in cracking process should not be neglected. In line with above, the highest contribution of non-acidic isolated Si-OH (3745 cm^{-1}) in deSi-0.5-ZSM-5 does not offer the significant advancement [29,30].

The presence of an Al-rich layer with many Lewis acid sites in deSi-
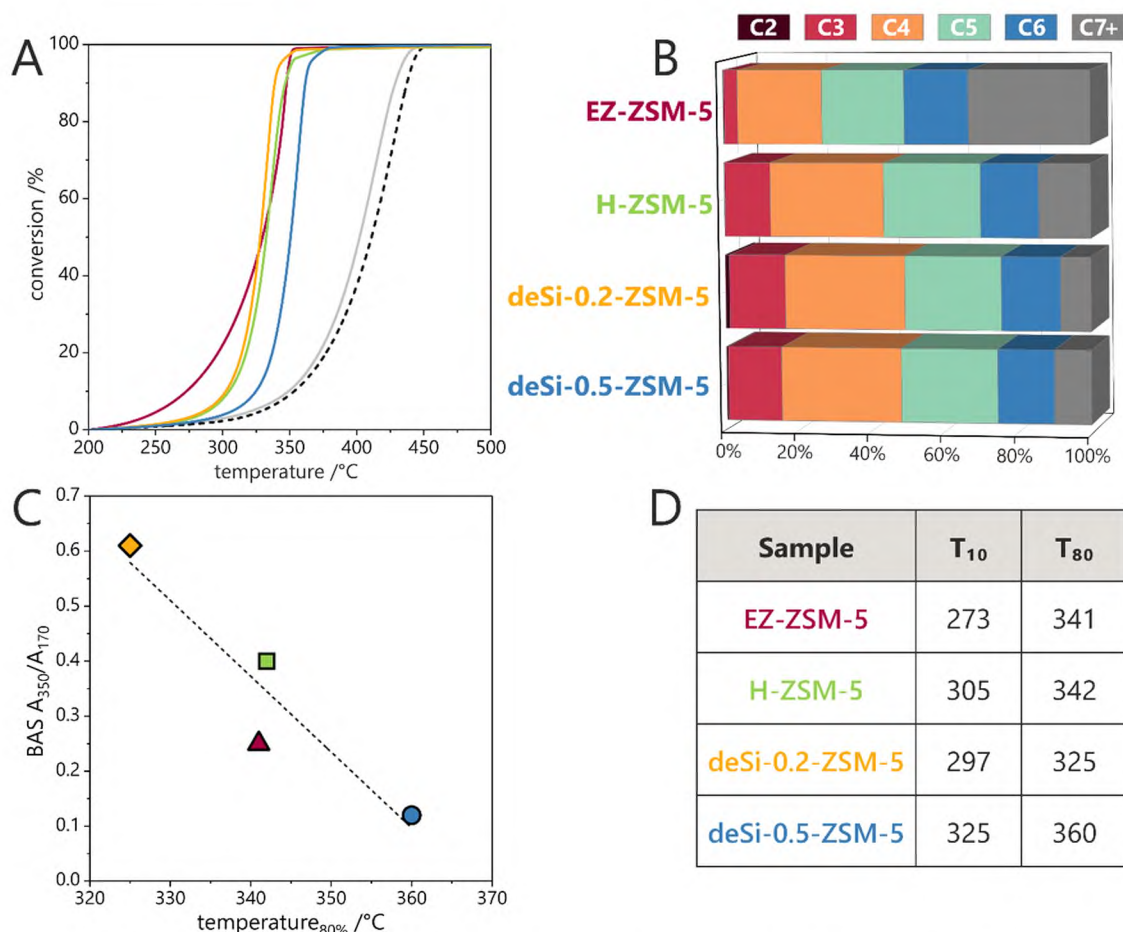
Fig. 5. (A) PP cracking (light-off diagrams) on EZ-ZSM-5, H-ZSM-5 and two hierarchical zeolites (deSi-0.2-ZSM-5 and deSi-0.5-ZSM-5, an "inert" SiO₂ (gray) and thermal cracking (dotted curve). (B) Product distribution from the catalytic PP cracking. C) T_{80} variation with BAS (A_{350}/A_{170} ratio). (D) Temperature for 10% and 80% conversion, T_{10} and T_{80}, respectively.

Sample	T_{10}	T_{80}
EZ-ZSM-5	273	341
H-ZSM-5	305	342
deSi-0.2-ZSM-5	297	325
deSi-0.5-ZSM-5	325	360

0.5-ZSM-5, Figs. 3 and 4, hampers the diffusion of reactants to the micropores. On deSi-0.2-ZSM-5, with a moderately developed mesopore surface area and low BAS density, the conversion above 350 °C is higher than for other catalysts. A similar critical role of LAS was previously reported by Tarach et al. [19]; a mild dealumination and redistribution of Al on the mesopore surface produces a more open hierarchical porosity. As a result, micropore mouths, free of LAS residues increase BAS accessibility as well as polymer cracking. Verboekend at al. [31] also reported inhibition of LDPE cracking on desilicated ITQ-4 at low conversion (10%) due to the presence of excessive amounts of Lewis acid sites.

At about 320 °C, PP conversion on EZ-ZSM-5 increases slower than on H-ZSM-5, indicating that BAS accessibility is not the only factor influencing catalyst performance. The linear dependence of T_{80} PP cracking and BAS strength (A_{350}/A_{170}) of crystalline zeolites highlights the influence of acidic strength on cracking activity at higher temperature range. On EZ-ZSM-5, the reduced acidic strength due to lower confinement is not compensated by a higher BAS accessibility. For instance, in *n*-decane cracking on zeolite Beta, BAS strength is the key factor determining catalytic activity [22]. In LDPE cracking, the porosity of hierarchical Beta zeolites helps when their BAS strength is above 80% of their pristine parent [32,33]. Fig. 5C and D therefore highlight that at low temperature, *i.e.* at low conversions, where the feedstock is mainly composed of very bulky molecules, active site accessibility is critical while at higher temperatures where reactants are less bulky molecules, "apparent acid strength" will play an increasing role.

The quantitative analysis of the PP cracking products by GC-MS shows that on the EZ-ZSM-5 catalyst less C_3-C_4 (gas) and C_5-C_6 (liquid), but more C_{7+} are produced compared to H-ZSM-5 and two hierarchical deSi-x-ZSM-5. It is therefore expected that a catalyst with a higher but less confined microporosity populated with BAS with lower strength will not favor secondary cracking. Moreover, on EZ-ZSM-5 more bimolecular reactions are expected due to the closer proximity of bulky reactants in larger cavities [34]. These observations are in line with literature reports [34,35] on the applicability of medium and wide pore zeolites in the catalytic degradation of polyethylene and polypropylene. The influence of the micropore volume, also impacts the side and sequential reactions and will appear later (Fig. 7).

The C_{4-5} product distribution highlights how the structural/textural and acidic properties influence PP cracking selectivity (Fig. 6). The hydrogen-transfer (HT) ability of zeolites is known to increase with micropore voids size and BAS density, in turn influencing the paraffin/olefin (p/o) ratio of the products [36,37]. DeSi-0.2-ZSM-5 and deSi-0.5-ZSM-5 zeolites display a lower HT and therefore produce more olefins in PP cracking. The large external surface and better acid sites accessibility in hierarchical catalysts limit the extent of secondary HT

reactions as those are favored by long reactions paths. This is the case for deSi-0.2-ZSM-5 producing the highest level of olefins. However, for deSi-0.5-ZSM-5, despite more macro- and meso-porosities, its higher BAS and LAS density promotes HT [38], therefore producing more paraffins. Moreover, LAS are also reported to interact with BAS to increase the acid strength of the latter (Table 2) [39,40].

EZ-ZSM-5 also increases isomerization (C_4 and C_5 fractions) following a bimolecular mechanism (HT reactions) in the more spacious voids of its partially formed unit cells. The high silanols population, which could possess some non-negligible acidity, *vide supra*, can also favor high *iso*-paraffin production. The inhibition of isomerization (an HT reaction) by shortening the reaction pathlength upon secondary intercrystalline or intracrystalline mesoporosity addition is observed on H-ZSM-5 and hierarchical samples. Corma et al. [41] reported that the Si/Al ratio determines the extent of bimolecular reactions by regulating carbenium ion residence times on the surface. The higher production of *iso*-C_4 and *iso*-C_5 paraffins in EZ-ZSM-5 could be ascribed to such a feature. Another source for higher p/o ratio is dehydrogenation reactions to aromatics all the way to coke [42], as the hydrogen produced can saturate olefins, albeit to a minor extent, as little hydrogen is available from such a route [38].

In PP cracking, EZ-ZSM-5 behaves more like a FAU than an MFI structure. In addition, some EZ-ZSM-5 acidic silanols could also play a role as already reported in zeolites for C_8-olefins and polypropylene [37]. The hierarchical deSi-0.2-ZSM-5 behaves as a zeolite with high acid strength, low acid site density, and microporous confinement leading to low initial conversions (low T) and limited HT. This results in lower p/o ratio and limited coke formation.

3.3. Polypropylene cracking and catalyst coking: 2D COS operando FT-IR spectroscopy

The above results are classically produced by relating catalyst characterization to their performances without inspecting the catalyst surface during the reaction. An *operando* study allows to go further and closer to the catalyst surface under realistic conditions of temperature and pressure. The 2D-COS IR technique is particularly suited as it correlates events taking place on the catalyst surface by looking simultaneously at active sites on the catalyst and reactants/products.

Time-resolved FT-IR, already proven helpful in hydrocarbon transformations [43,44] is applied here to monitor simultaneously PP cracking and the catalyst surface (Fig. 7). By following the $A\nu(-CH_3)/A\nu(-CH_2)$ PP ratio evolution during reaction, where $A\nu(-CH_3)$ and $A\nu(-CH_2)$ represent the intensities of the of $-CH_3$ (2960 cm^{-1}) and $-CH_2-$ (2925 cm^{-1}) bands characteristic for the surface adsorbed species, the influence of the different catalysts is evidenced. The CH_2/CH_3 intensity
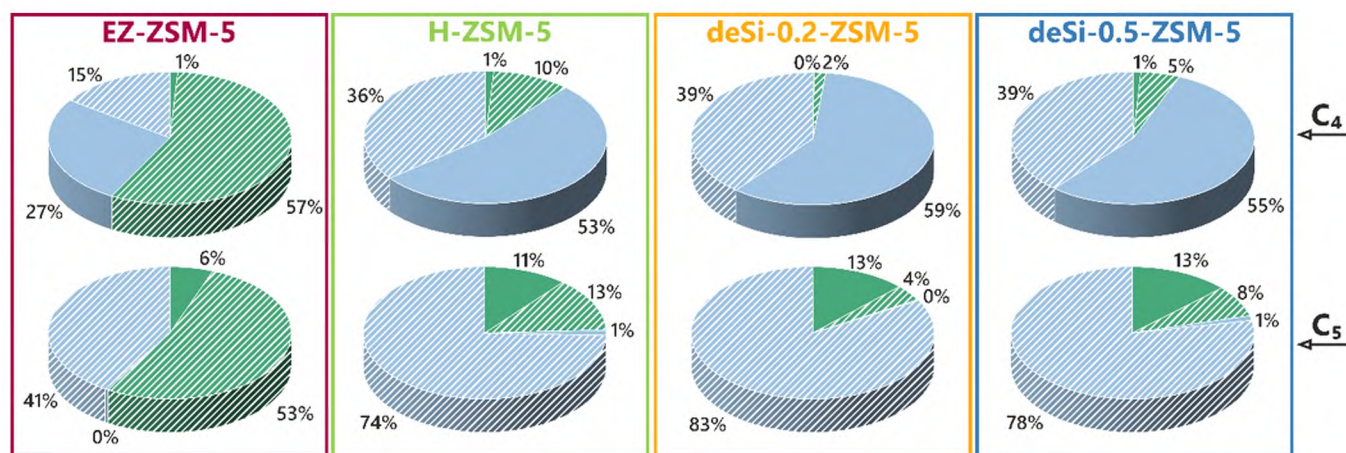
Fig. 6. Cracking products distribution in C_4 and C_5 fractions: paraffinic (green), olefinic (blue), branched (hatched), and linear (filled).
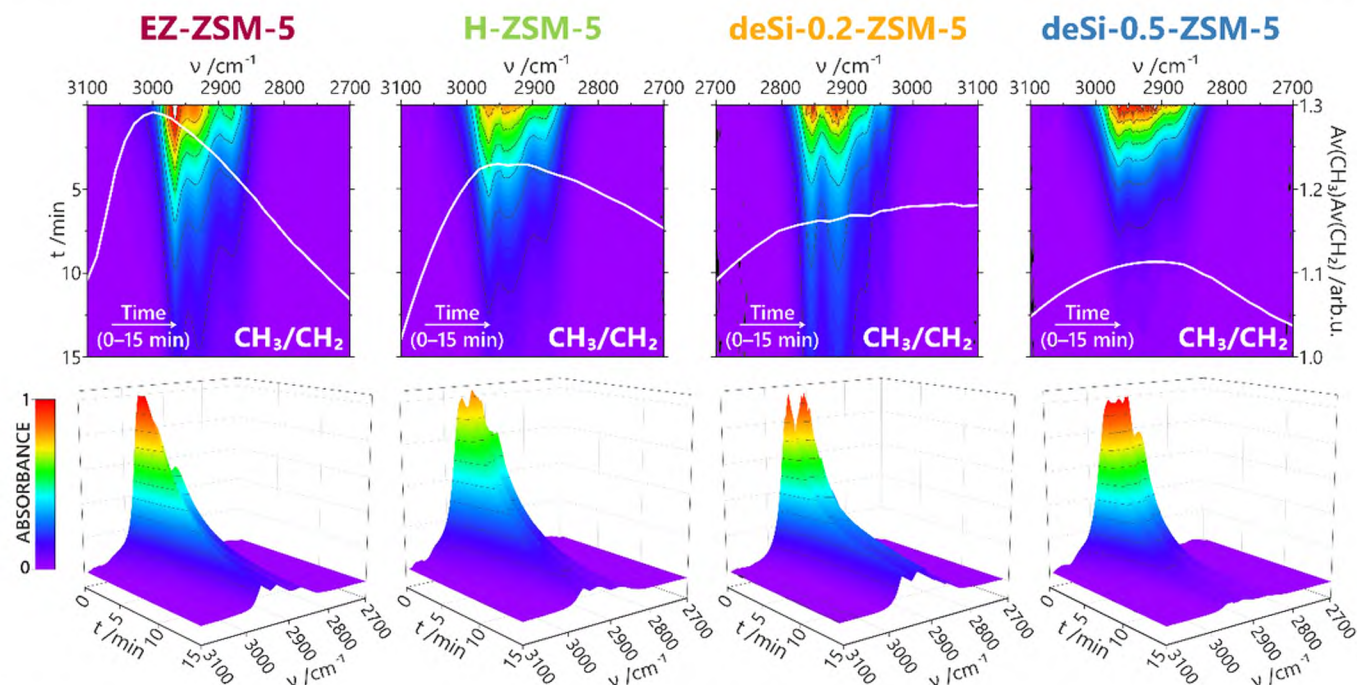
Fig. 7. Top-projection of 3-D maps (bottom row) of the evolution of C–H stretching band intensity within 15 min of PP cracking. The white curve (top row) represents changes in the CH_3/CH_2 bands area ratio.

ratio is widely used to estimate the length and degree of branching of the aliphatic side-chains; the larger this ratio, the longer the aliphatic chain [45–47]. EZ-ZSM-5 is the most active in end-chain cracking at the earliest stages of the reaction (0–3 min), goes through a maximum before decreasing rapidly due to the formation and retention of heavy by-products (coke precursors), leading to deactivation. Such a deactivation step is not observed on deSi-0.2-ZSM-5 where the $A\nu(-CH_3)/A\nu(-CH_2)$ ratio decrease is minimal, and a high proportion of light hydrocarbons is produced.

The cracking efficiency is easily seen on 2D COS maps (Fig. 8A). The positive cross-peaks on 2D COS maps, spreading from $1475 - 1425$ cm^{-1} and $1383 - 1345$ cm^{-1} are more intense on the X-ray amorphous EZ-ZSM-5 than on the other crystalline catalysts where cross-peaks are centered at 1461 and 1383 cm^{-1}. The positive correlation between the CH_3 and CH_2 deformation bands at *ca.* 1461 and 1383 cm^{-1} evidence PP decomposition on the catalysts. A single band developing at 1383 cm^{-1} is associated with the $\delta_s(CH_3)$ mode, whereas the peaks at 1360 and 1345 cm^{-1} witness the appearance of branched $-CH(CH_3)_2$ and $-C(CH_3)_3$ terminations [48]. As the intensity of the CH_3 deformation bands is always higher than CH_2, the formation of the $CH_3(CH_2)_2CH_2^+$ species is proposed. This further supports the formation of more branched products of partially cracked PP chains on EZ-ZSM-5, while on all other zeolites the linear fragments dominate. Summing up, embryonic zeolites are more active in PO cracking as the higher accessibility of their acid sites more than compensates their lower concentration and strength. Higher bimolecular reaction rate in their supermicropores provides a distinct selectivity to branched hydrocarbons. Contrarily, in desilicated zeolites transition states are not confined and stabilized by van der Waals interactions in mesopores and display lower rates in acid-catalyzed PO cracking reactions.

The accumulation of coke precursors on 2D COS maps (Fig. 8A) appears as a negative correlation between $CH_3/-CH_2$ deformation bands (1461/1383 cm^{-1}) and the complex C=C stretching band (1620–1580 cm^{-1}). A sequence of catalytic events can be derived from a mutual analysis of synchronous (Fig. 8A) and asynchronous maps (Fig. 8B). The product of asynchronous and synchronous sets (synchronous × asynchronous) is one of the straightforward insight into the

interplay between the cracking and coking processes (Fig. 8C). The analysis of the product maps is still based on the principles given by Noda [49]. In EZ-ZSM-5 the first coke precursor is identified by the $\nu_{(C=C)ring}$ band at 1544 cm^{-1}, typical of polyolefins and methyl-substituted benzyl cations or polycyclic aromatics characterized by the band centered at 1600–1590 cm^{-1} [43,44]. The differentiated intensity of the peaks in product maps related to the CH_3 and CH_2 deformation region, *i.e.*, 1470–1300 cm^{-1}, indicates that PP cracking mechanism is ruled by the acidic and textural properties of the catalysts. The band near 1480–1430 cm^{-1} is associated with an asymmetric out-of-plane CH_3 deformation, while the *ca.* 1393–1356 cm^{-1} represents a symmetric in-phase CH_3 deformations. When two methyls are bound to one saturated carbon in isopropyl or gem-dimethyl groups, two bands with nearly equal intensity appear at 1385 and 1368 cm^{-1} [50]. The 1330 cm^{-1} band belongs to a C—H bending mode (C_3CH). The most complex picture of CH_3 and CH_2 vibrations is representative of EZ-ZSM-5 and the absence of tertiary C—H bending mode indicates the preservation of longer chains of PP on the EZ-ZSM-5 surface. From the sequential order of events, it can be anticipated that the coke precursors formations (1620–1580 cm^{-1}) are continuously integrated with polymer cracking on EZ-ZSM-5. In contrast, H-ZSM-5 and deSi-0.5-ZSM-5 activate the cyclization and aromatization processes which precede the cracking of PP; the dominant coke precursors bands are gathered in the 1650–1580 cm^{-1} spectral region. In deSi-0.2-ZSM-5, the ultimate processing of PP is coking of the catalyst, as identified by the formation of trisubstituted aromatics and/or polycyclic aromatics to a significant extent (1625–1600 cm^{-1}). The catalyst-coking susceptibility is discussed further later.

3.4. Coke burn-off: thermogravimetry and operando FT IR-TPO-MS

As coke deactivation of a catalyst changes its activity and selectivity, understanding the related hydrogen transfer processes is important. An earlier scheme [51] describes successive oligomerization, cyclization, and dehydrogenation of small molecules on active sites located in zeolite pores: alkanes - alkenes - oligomers - naphthenes - aromatics - coke. The time evolution of the $A\nu(-CH_3)/A\nu(-CH_2)$ in Fig. 7, indicates that
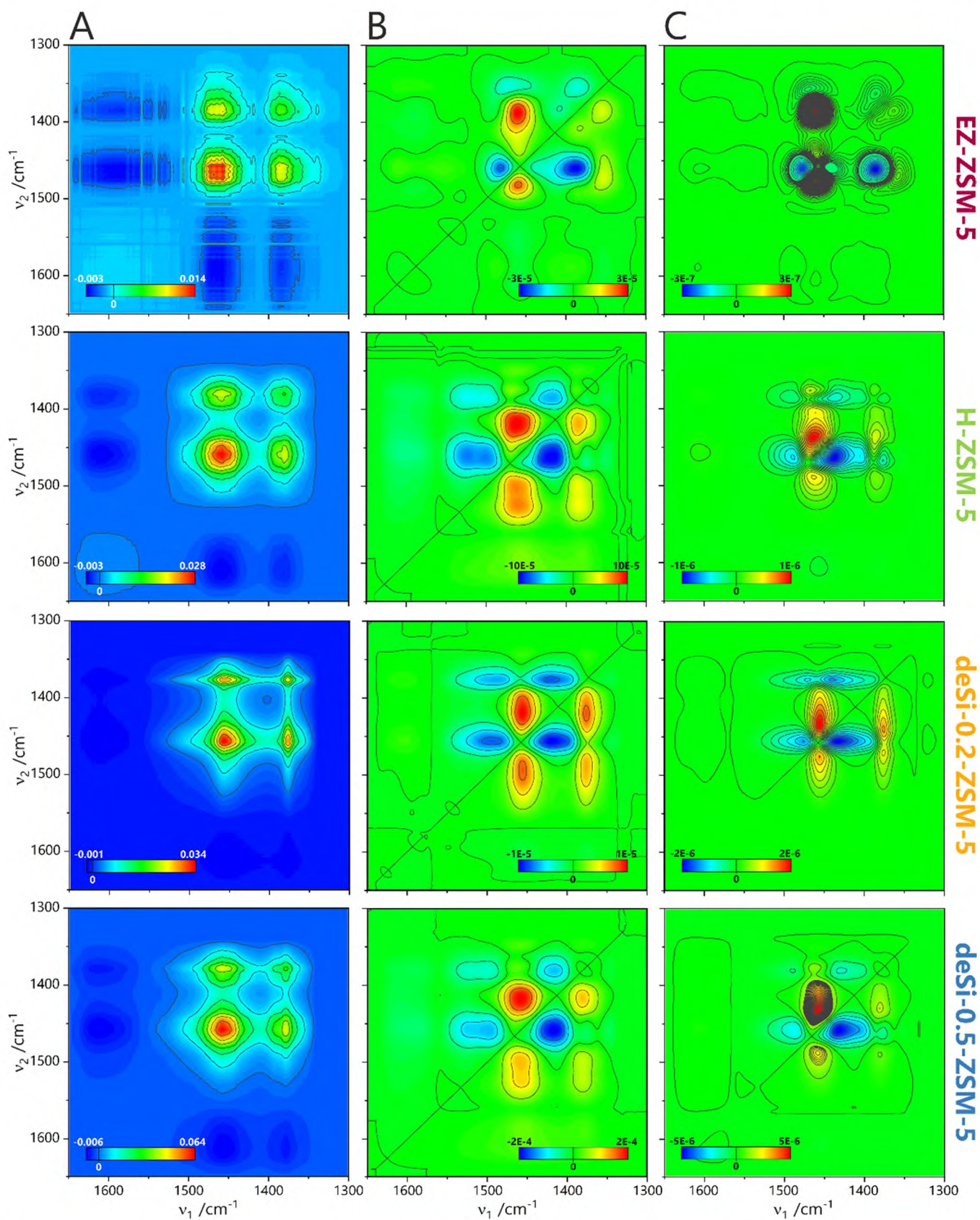
Fig. 8. 2D COS IR synchronous (A), asynchronous (B) maps and their product (synchronous × asynchronous) (C) illustrating coke formation during PP cracking. The color coding (inset) represents correlation levels between the respective bands.

hierarchical zeolites (deSi-0.5-ZSM-5 and deSi-0.2-ZSM-5) exhibit lower coke formation and slower deactivation. This is due to an easier transport of reactants in the zeolites as well as a lowering of diffusional restrictions on secondary products. The FT-IR 2D COS maps of the PP cracking (Fig. 8) indicate a correlation between polymer chains cracking and the simultaneous formation of unsaturated non-volatile high-carbon species identified by the cross peaks in the $1650 - 1570$ cm^{-1} region (maximum at *ca.* 1605 cm^{-1}). This implies that in H-ZSM-5 and deSi-ZSM-5 zeolites, coke consists of both methyl-substituted cyclo-alkenyl carbenium ions species, methyl-substituted benzene cations or polycyclic aromatic compounds. Thus a high number of strong BAS promotes condensations and aromatizations [43,52,53]. On EZ-ZSM-5, coke species are more diverse, as in addition to the 1605 cm^{-1} species, bands in the $1565 - 1525$ cm^{-1} region attest the presence of alkyl aromatics (alkylbenzenes) and conjugated olefinic species $(C_nH_{2n+1})^+$ [54,55]. The microporous structure of EZ-ZSM-5 reduces the heavy coke fractions.

Coke combustion under air is a common procedure to evaluate its nature and of course to regenerate an industrial catalyst. The amount of coke estimated from TGA (Fig. 9) is higher on EZ-ZSM-5 (5.5%) than on H-ZSM-5 (1.4%), and the hierarchical deSi-0.2-ZSM-5 (2.1%) and deSi-0.5-ZSM-5 (1.15%). It is related to the coking rates observed on the time evolution of the $A\nu(-CH_3)/A\nu(-CH_2)$ ratio (Fig. 7), where EZ-ZSM-5 is the highest. Coke oxidation starts on molecules located on the catalyst external surface and then progresses inside the micropores, where oxygen availability becomes key. So, coke on EZ-ZSM-5 burns more rapidly than on H-ZSM-5 and deSi-ZSM-5. As the 2D COS IR analysis already showed that coke species on EZ-ZSM-5 are more diverse, this accounts for the three steps (450–555 °C) observed in its light-off curve (Fig. 8). Magnoux and Guisnet [56] already concluded that both coking and coke oxidation are shape-selective reactions. It is commonly agreed that in MFI-type zeolite, carbonaceous compounds formed at channel intersections totally block oxygen diffusion during regeneration. On large pore zeolites such as FAU and MOR, oxygen can still diffuse in their micropores. So, despite extensive coking on EZ-ZSM-5, an efficient contact between reactants (coke and oxygen) facilitates regeneration. In deSi-0.2-ZM-5, the denser coke located on its external surface is removed at higher temperatures. The internal coke on deSi-0.2-ZSM-5 burns at still higher temperatures pointing to slow oxygen diffusion in micropores blocked by carbonaceous residues at channel intersections. This result confirms the high toxicity of coke on desilicated zeolites compared to embryonic ones. The high micropore volume of EZ-ZSM-5 combined with a low Brønsted acidity prevents coke precursors to evolve into heavy toxic coke as found on the crystalline zeolites.
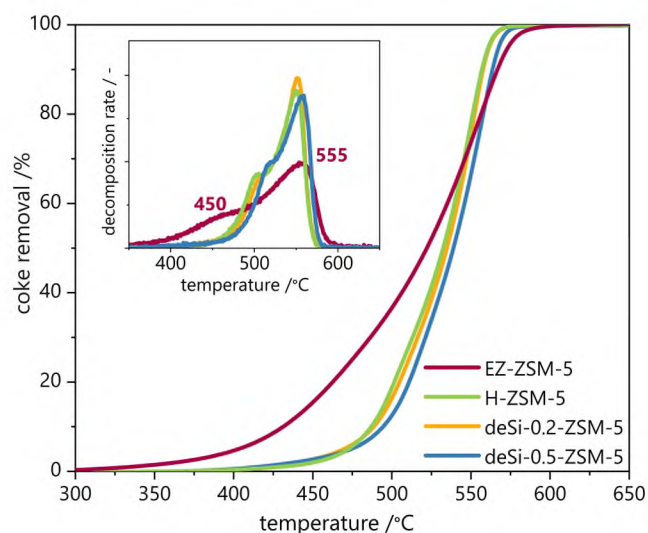
On deSi-0.2-ZSM-5, stronger retention of coke and its precursors is favored by the presence of stronger acid sites. Carbenium ions adsorbed in zeolite micropores are stabilized by framework oxygens, acting as weak bases conjugated with the strong acid sites. Such carbenium ions are less susceptible to desorption as this requires a proton abstraction the carbenium ion, impossible on a weak base. The long residence time of carbenium ions in deSi-0.2-ZSM-5 contributes to coke formation by oligomerization, elimination, and ion-ion disproportionation. On deSi-0.5-ZSM-5, a lower Si/Al produces framework oxygen of higher basicity, reducing the rate of bimolecular reactions between adjacent ions by enhancing proton abstraction from the carbenium ion and hence a desorption of olefins (*cf.* selectivities on Fig. 6). This effect is more significant than faster diffusion resulting from the greater mesoporosity of deSi-0.5-ZSM-5. In the case of EZ-ZSM-5 more coking and significantly higher production of *iso*-C_4 and *iso*-C_5 paraffins indicate faster hydrogen, not due to a higher BAS strength but by the more open voids in EZ-ZSM-5, akin to those found in extra-large microporous materials. This nature of coke in EZ-ZSM-5 is detailed in their TGA profiles, and IR explains its removal by combustion.

Silanols also impact catalyst deactivation, as observed on EZ-ZSM-5 and deSi-0.2-ZSM-5, the two materials with the highest population. The highest level of coke observed is on EZ-ZSM-5 where internal silanols are predominant, while on deSi-0.2-ZSM-5 with external silanols, coke and deactivation are lower. It highlights further that different types of silanols have a direct influence on coke formation and its preferential location on the most acidic silanols, as observed elsewhere [37]. While in mildly hierarchical deSi-0.2-ZSM-5 coking is driven by strong BAS located in the native microporosity, in X-ray amorphous EZ-ZSM-5, acidic internal silanols and a higher microporosity promote a higher degree of coking.

Further information on the coke nature is provided during an *operando* IR-TPO-MS monitoring of coke removal (Fig. 10). CO_2 and H_2O formed during the temperature-programmed oxidation (TPO, 5% of O_2 in N_2) of carbonaceous species are monitored by mass spectrometry. TPO is performed at 300, 350, 400, 450, 500, and 550 °C; at each temperature, a 10 min isotherm step is maintained before increasing the temperature further at a rate of 10 °C/min. Only the corresponding 2D COS IR maps highlighting changes in spectral features during regeneration at 300 °C and 500 °C are discussed further (Fig. 10). In the case of catalysts with high microporosity, H-ZSM-5 and EZ-ZSM-5, H_2O ($m/z = 18$) production is maintained throughout the process and greatly exceeds CO_2 production. On the hierarchical zeolites, deSi-0.2-ZSM-5 and deSi-0.5-ZSM-5, less H_2O is produced at a slightly higher level than CO_2. The high level of water production in the first stages of the TPO is associated with the burning of unreacted PP (conversion under isothermal *operando* conditions at 250 °C does not reach 100%). This is illustrated on 2D COS IR maps of coke combustion at 300 °C. The observed correlations between the C=C stretching modes (1605 cm^{-1}) and asymmetric (1425 cm^{-1}) or symmetric modes of alkyl groups (1340 cm^{-1}) in aliphatics and alkyl aromatics indicates the presence of hydrocarbons with high H/C on the external surface of H-ZSM-5 and EZ-ZSM-5. For deSi-0.5-ZSM-5 and deSi-0.2-ZSM-5, with added intracrystalline mesoporosity, a much lower H_2O/CO_2 ratio is observed during the entire TPO, indicating coke with lower H/C is combusted. The 2D COS IR maps of desi-0.5-ZSM-5 and desi-0.2-ZSM-5 do not show any significant correlation between C=C and alkyl vibration during combustion at 300 °C. The CO_2 and H_2O production in the final stages of coke combustion is constant on all the catalysts, albeit significantly higher for EZ-ZSM-5 and H-ZSM-5. This also appears in the 2D COS IR maps during coke oxidation at 500 °C (Fig. 10). The patterns in the synchronous spectrum of the CH_3 and CH_2 deformation modes (1380 –1340 cm^{-1}) are referred to as "*angel*" patterns with cross peak wings. They appear when bands shift to higher frequencies together with some intensity increase, usually the result of recording spectra at increasing temperatures. In our case, since temperature remains constant, temperature-induced shift of the CH_3 band can be excluded. Such

Fig. 9. Coke light-off curves and their derivatives (inset).
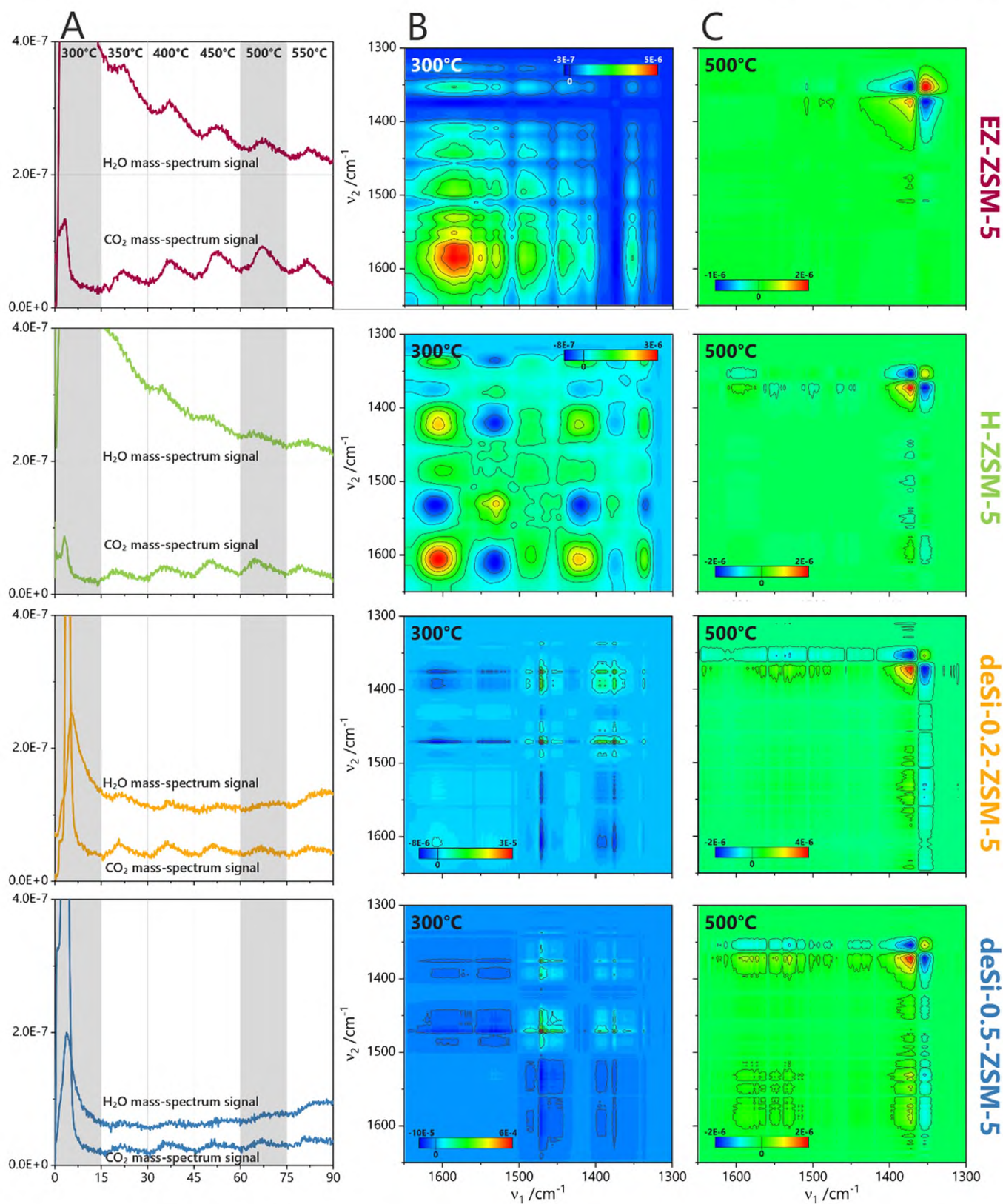
Fig. 10. TPO of coked catalysts illustrated as the mass signal intensity of the CO_2 ($m/z = 44$) and H_2O ($m/z = 18$) evolved gases at increasing temperatures (A). 2D COS IR synchronous maps of correlated events during coke oxidation at 300 °C (B) and 500 °C (C). The color coding represents the correlation between the respective bands (insets).

angel patterns are thus not artifacts but reflect complex spectral changes in position and line shape of IR bands related to coke species. All changes are, therefore, due to the interaction of oxygen with the carbonaceous species. The angel pattern involves terminal CH_3 symmetric mode (1383 cm^{-1}) and branched $-CH(CH_3)_2$ and $-C(CH_3)_3$ terminations (1360 and 1345 cm^{-1}, resp.). A longer contact time between the spent catalyst and oxygen increases the conversion of $-CH_3$ from branched ramifications to terminal isolated methyl groups. Independently from the catalyst, coke oxidation is therefore initiated on methyl groups forming oxygenated intermediates further decomposed into CO_2.

Correlation peaks are observed between polyaromatics (the $C=C$ stretching modes at 1605 cm^{-1}) and methyl groups (1400 -1325 cm^{-1}) in H-ZSM-5 and hierarchical materials, while no such correlation appear in the with EZ-ZSM-5; only very weak correlations between aliphatics and conjugated olefins (1525 -1480 cm^{-1}) appear. While in H-ZSM-5 and mesoporous deSi-0.2-ZSM-5 and deSi-0.5-ZSM-5 coke oxidation are initiated on the $-CH(CH_3)_2$ and $-C(CH_3)_3$ groups on aromatic rings, on EZ-ZSM-5 oxidation starts on alkyl species, as the aliphatics decrease independently of the coke.

4. Conclusions

This study highlights the complexity of a model polyolefin (PO), pure polypropylene, cracking on various forms of the H-ZSM-5 zeolite, namely embryonic, purely microporous, and hierarchical. Two zeolite parameters play complementary roles: porosity, and acid site strength related to confinement. Our paper shows that FCC type of catalysts are a good basis to design a PO depolymerization process. Highly accessible acid sites in EZ-ZSM-5 are required to attack the bulky polymer and protons confined in micropores take advantage to bimolecular reactions to fine-tune selectivity towards final products. Therefore, we need to work with well-defined and controlled catalysts to understand the mode of action of poorly described FCC catalysts (the patented preparations are never mentioned in the open literature when commercial FCC catalysts are used to crack PO).

The complexity is also a source of opportunities to design catalysts dedicated to the chemical recycling of polyolefins in an FCC type of process. The rapid but reversible catalyst deactivation followed by its regeneration makes PP chemical recycling to fuel or petrochemical possible in existing and already optimized FCC units.

The overall methodology sheds light on the chemistry of the process, including catalyst regeneration. The relative role of the microporous and mesoporous surfaces of zeolites are highlighted and the *operando* FT-IR study can be used at two levels: 1) understanding the fundamentals of the intricate catalyst reactants/products interactions during the reaction, and 2) fingerprinting the catalyst behavior to better optimize its design. The evaluation of the processing of PO in FCC should not be limited to MFI type zeolites, but others like FAU (used in current FCC catalysts), BEA… should be considered or mixtures thereof. It is probable that if such catalytic PO recycling takes place in existing or grass-root FCC units, many options exist to fine-tune the design of drop-in catalysts by combining the presence of various zeolites or amorphous components, as already practiced in the processing of heavy and highly polluted oil fractions [4]. As in the current FCC operations, the heat requirements of the (endothermic) cracking can be met by the (exothermic) coke combustion with the catalyst microspheres playing the role of the heat transfer fluid.

CRediT authorship contribution statement

Karolina Tarach: Methodology, Investigation, Validation, Data Curation, Writing - Review & Editing. **Mariame Akouche**: Investigation; Data curation. **Kamila Pyra**: Investigation; Data curation. **Valentin Valtchev**: Writing - Review & Editing. **Gabriela Jajko**: Data curation, Visualization. **Kinga Góra-Marek**: Conceptualization, Project administration, Funding acquisition, Writing - Original Draft, Writing -

Review & Editing. **Jean-Pierre Gilson**: Writing - Original Draft, Writing - Review & Editing.

Declaration of Competing Interest

The authors declare that they have no known competing financial interests or personal relationships that could have appeared to influence the work reported in this paper.

Data availability

I have shared the link to my data in the Attach File step.
Polypropylene cracking on embryonic and ZSM-5 catalysts (Original data) (Jagiellonian University Repository)

Acknowledgments

References

[1] T. Hundertmark, C. McNally, T.J. Simons, H. Vanthournout, No time to waste: what plastics recycling could offer, McKinsey Chem, 2018. ⟨https://doi.org/ https://www.mckinsey.com/industries/chemicals/our-insights/no-time-to-waste-what-plastics-recycling-could-offer⟩.
[2] Y. Wang, Y. Zhang, H. Fan, P. Wu, M. Liu, X. Li, J. Yang, C. Liu, P. Bai, Z. Yan, Elucidating the structure-performance relationship of typical commercial zeolites in catalytic cracking of low-density polyethylene, Catal. Today 405–406 (2022) 135–143, https://doi.org/10.1016/J.CATTOD.2022.06.024.
[3] Y.H. Seo, K.H. Lee, D.H. Shin, Investigation of catalytic degradation of high-density polyethylene by hydrocarbon group type analysis, J. Anal. Appl. Pyrolysis 70 (2003) 383–398, https://doi.org/10.1016/S0165-2370(02)00186-9.
[4] W. Vermeiren, J.-P. Gilson, Impact of zeolites on the petroleum and petrochemical industry, Top. Catal. 52 (2009) 1131–1161, https://doi.org/10.1007/s11244-009-9271-8.
[5] S. Mintova, J.-P. Gilson, V. Valtchev, Advances in nanosized zeolites, Nanoscale 5 (2013) 6693–6703, https://doi.org/10.1039/C3NR01629C.
[6] K.-G. Haw, J.-M. Goupil, J.-P. Gilson, N. Nesterenko, D. Minoux, J.-P. Dath, V. Valtchev, Embryonic ZSM-5 zeolites: zeolitic materials with superior catalytic activity in 1,3,5-triisopropylbenzene dealkylation, New J. Chem. 40 (2016) 4307–4313, https://doi.org/10.1039/C5NJ03310A.
[7] K.-G. Haw, J.-P. Gilson, N. Nesterenko, M. Akouche, H. El Siblani, J.-M. Goupil, B. Rigaud, D. Minoux, J.-P. Dath, V. Valtchev, Supported embryonic zeolites and their use to process bulky molecules, ACS Catal. 8 (2018) 8199–8212, https://doi.org/10.1021/acscatal.8b01936.
[8] M. Akouche, J.-P. Gilson, N. Nesterenko, S. Moldovan, D. Chateigner, H. El Siblani, D. Minoux, J.-P. Dath, V. Valtchev, Synthesis of embryonic zeolites with controlled physicochemical properties, Chem. Mater. 32 (2020) 2123–2132, https://doi.org/10.1021/acs.chemmater.9b05258.
[9] A. Palčić, S.N. Jaén, D. Wu, M. Cai, C. Liu, E.A. Pidko, A.Y. Khodakov, V. Ordomsky, V. Valtchev, Embryonic zeolites for highly efficient synthesis of dimethyl ether from syngas, Microporous Mesoporous Mater. 322 (2021), 111138, https://doi.org/10.1016/J.MICROMESO.2021.111138.
[10] D. Verboekend, S. Mitchell, M. Milina, J.C. Groen, J. Pérez-Ramírez, Full compositional flexibility in the preparation of mesoporous MFI zeolites by desilication, J. Phys. Chem. C 115 (2011) 14193–14203, https://doi.org/10.1021/jp201671s.
[11] K. Sadowska, K. Góra-Marek, J. Datka, Hierarchic zeolites studied by IR spectroscopy: acid properties of zeolite ZSM-5 desilicated with NaOH and NaOH/tetrabutylamine hydroxide, Vib. Spectrosc. 63 (2012) 418–425, https://doi.org/10.1016/J.VIBSPEC.2012.09.007.
[12] K. Góra-Marek, K. Tarach, M. Choi, 2,6-Di-tert-butylpyridine sorption approach to quantify the external acidity in hierarchical zeolites, J. Phys. Chem. C 118 (2014) 12266–12274, https://doi.org/10.1021/jp501928k.

[13] M. Thommes, K. Kaneko, A.V. Neimark, J.P. Olivier, F. Rodriguez-Reinoso, J. Rouquerol, K.S.W. Sing, Physisorption of gases, with special reference to the evaluation of surface area and pore size distribution (IUPAC technical report), Pure Appl. Chem. 87 (2015) 1051–1069, https://doi.org/10.1515/pac-2014-1117.

[14] C. Schlumberger, M. Thommes, Characterization of hierarchically ordered porous materials by physisorption and mercury porosimetry—a tutorial review, Adv. Mater. Interfaces 8 (2021), 2002181, https://doi.org/10.1002/admi.202002181.

[15] K.A. Tarach, K. Góra-Marek, J. Martinez-Triguero, I. Melián-Cabrera, Acidity and accessibility studies of desilicated ZSM-5 zeolites in terms of their effectiveness as catalysts in acid-catalyzed cracking processes, Catal. Sci. Technol. 7 (2017) 858–873, https://doi.org/10.1039/C6CY02609E.

[16] K. Góra-Marek, M. Derewiński, P. Sarv, J. Datka, IR and NMR studies of mesoporous alumina and related aluminosilicates, Catal. Today 101 (2005) 131–138, https://doi.org/10.1016/J.CATTOD.2005.01.010.

[17] I.C. Medeiros-Costa, E. Dib, N. Nesterenko, J.-P. Dath, J.-P. Gilson, S. Mintova, Silanol defect engineering and healing in zeolites: opportunities to fine-tune their properties and performances, Chem. Soc. Rev. 50 (2021) 11156–11179, https://doi.org/10.1039/D1CS00395J.

[18] L. Lakiss, C. Kouvatas, J.-P. Gilson, V. Valtchev, S. Mintova, C. Fernandez, R. Bedard, S. Abdo, J. Bricker, Atomic-insight into zeolite catalyst forming—an advanced NMR study, J. Phys. Chem. C 125 (2021) 20028–20034, https://doi.org/10.1021/acs.jpcc.1c05501.

[19] K.A. Tarach, K. Pyra, K. Góra-Marek, Opening up ZSM-5 hierarchical zeolite's porosity through sequential treatments for improved low-density polyethylene cracking, Molecules 25 (2020), https://doi.org/10.3390/molecules25122878.

[20] K. Khivantsev, N.R. Jaegers, L. Kovarik, M.A. Derewinski, J.-H. Kwak, J. Szanyi, On the nature of extra-framework aluminum species and improved catalytic properties in steamed zeolites, Molecules 27 (2022), https://doi.org/10.3390/molecules27072352.

[21] N.S. Nesterenko, F. Thibault-Starzyk, V. Montouilliout, V.V. Yushchenko, C. Fernandez, J.-P. Gilson, F. Fajula, I.I. Ivanova, The use of the consecutive adsorption of pyridine bases and carbon monoxide in the IR spectroscopic study of the accessibility of acid sites in microporous/mesoporous materials, Kinet. Catal. 47 (2006) 40–48, https://doi.org/10.1134/S0023158406010071.

[22] K. Tarach, K. Góra-Marek, J. Tekla, K. Brylewska, J. Datka, K. Mlekodaj, W. Makowski, M.C. Igualada López, J. Martínez Triguero, F. Rey, Catalytic cracking performance of alkaline-treated zeolite Beta in the terms of acid sites properties and their accessibility, J. Catal. 312 (2014) 46–57, https://doi.org/10.1016/J.JCAT.2014.01.009.

[23] M. Boronat, A. Corma, What is measured when measuring acidity in zeolites with probe molecules? ACS Catal. 9 (2019) 1539–1548, https://doi.org/10.1021/acscatal.8b04317.

[24] A. Primo, H. Garcia, Zeolites as catalysts in oil refining, Chem. Soc. Rev. 43 (2014) 7548–7561, https://doi.org/10.1039/C3CS60394F.

[25] J. Dwyer, F.R. Fitch, E.E. Nkang, Dependence of zeolite properties on composition. Unifying concepts, J. Phys. Chem. 87 (1983) 5402–5404, https://doi.org/10.1021/j150644a019.

[26] K. Góra-Marek, I. Melián-Cabrera, A note on the acid strength of porous materials assessed by thermal methods, Microporous Mesoporous Mater. 310 (2021), 110638, https://doi.org/10.1016/j.micromeso.2020.110638.

[27] I.C. Medeiros-Costa, E. Dib, F. Dubray, S. Moldovan, J.-P. Gilson, J.-P. Dath, N. Nesterenko, H.A. Aleksandrov, G.N. Vayssilov, S. Mintova, Unraveling the effect of silanol defects on the insertion of single-site Mo in the MFI zeolite framework, Inorg. Chem. 61 (2022) 1418–1425, https://doi.org/10.1021/acs.inorgchem.1c03076.

[28] A.B. Fernández, I. Lezcano-Gonzalez, M. Boronat, T. Blasco, A. Corma, NMR spectroscopy and theoretical calculations demonstrate the nature and location of active sites for the Beckmann rearrangement reaction in microporous materials, J. Catal. 249 (2007) 116–119, https://doi.org/10.1016/J.JCAT.2007.03.030.

[29] L. Dalstein, E. Potapova, E. Tyrode, The elusive silica/water interface: isolated silanols under water as revealed by vibrational sum frequency spectroscopy, Phys. Chem. Chem. Phys. 19 (2017) 10343–10349, https://doi.org/10.1039/C7CP01507K.

[30] E. Dib, I.M. Costa, G.N. Vayssilov, H.A. Aleksandrov, S. Mintova, Complex H-bonded silanol network in zeolites revealed by IR and NMR spectroscopy combined with DFT calculations, J. Mater. Chem. A 9 (2021) 27347–27352, https://doi.org/10.1039/D1TA06908J.

[31] D. Verboekend, J.C. Groen, J. Pérez-Ramírez, Interplay of properties and functions upon introduction of mesoporosity in ITQ-4 zeolite, Adv. Funct. Mater. 20 (2010) 1441–1450, https://doi.org/10.1002/adfm.200902205.

[32] K. Pyra, K.A. Tarach, E. Janiszewska, D. Majda, K. Góra-Marek, Evaluation of the textural parameters of zeolite beta in LDPE catalytic degradation: thermogravimetric analysis coupled with FTIR operando studies, Molecules 25 (2020), https://doi.org/10.3390/molecules25040926.

[33] K. Pyra, K.A. Tarach, D. Majda, K. Góra-Marek, Desilicated zeolite BEA for the catalytic cracking of LDPE: the interplay between acidic sites' strength and accessibility, Catal. Sci. Technol. 9 (2019) 1794–1801, https://doi.org/10.1039/C9CY00326F.

[34] G. Manos, A. Garforth, J. Dwyer, Catalytic degradation of high-density polyethylene over different zeolitic structures, Ind. Eng. Chem. Res. 39 (2000) 1198–1202, https://doi.org/10.1021/ie990512q.

[35] Q. Zhou, L. Zheng, Y.Z. Wang, G.M. Zhao, B. Wang, Catalytic degradation of low-density polyethylene and polypropylene using modified ZSM-5 zeolites, Polym. Degrad. Stab. 84 (2004) 493–497, https://doi.org/10.1016/J.POLYMDEGRADSTAB.2004.01.007.

[36] K. Pyra, K.A. Tarach, K. Góra-Marek, Towards a greater olefin share in polypropylene cracking – amorphous mesoporous aluminosilicate competes with zeolites, Appl. Catal. B Environ. 297 (2021), 120408, https://doi.org/10.1016/J.APCATB.2021.120408.

[37] B. Reiprich, K.A. Tarach, K. Pyra, G. Grzybek, K. Góra-Marek, High-silica layer-like zeolites Y from seeding-free synthesis and their catalytic performance in low-density polyethylene cracking, ACS Appl. Mater. Interfaces 14 (2022) 6667–6679, https://doi.org/10.1021/acsami.1c21471.

[38] K.A. Cumming, B.W. Wojciechowski, Hydrogen transfer, coke formation, and catalyst decay and their role in the chain mechanism of catalytic cracking, Catal. Rev. 38 (1996) 101–157, https://doi.org/10.1080/01614949608006455.

[39] S. Li, A. Zheng, Y. Su, H. Zhang, L. Chen, J. Yang, C. Ye, F. Deng, Brønsted/Lewis acid synergy in dealuminated HY zeolite: a combined solid-state NMR and theoretical calculation study, J. Am. Chem. Soc. 129 (2007) 11161–11171, https://doi.org/10.1021/ja072767y.

[40] M. Derewiński, K. Góra-Marek, K. Lázár, J. Datka, Nature of active sites in the Fe-TON Zeolites: Mössbauer and IR studies, Stud. Surf. Sci. Catal. 174 (2008) 865–868, https://doi.org/10.1016/S0167-2991(08)80025-0.

[41] A. Corma, P.J. Miguel, A.V. Orchillés, The role of reaction temperature and cracking catalyst characteristics in determining the relative rates of protolytic cracking, chain propagation, and hydrogen transfer, J. Catal. 145 (1994) 171–180, https://doi.org/10.1006/JCAT.1994.1020.

[42] J. Abbot, B.W. Wojciechowski, Catalytic reactions of branched paraffins on HY zeolite, J. Catal. 113 (1988) 353–366, https://doi.org/10.1016/0021-9517(88)90264-3.

[43] K. Gołąbek, K.A. Tarach, K. Góra-Marek, Standard and rapid scan infrared spectroscopic studies of o-xylene transformations in terms of pore arrangement of 10-ring zeolites – 2D COS analysis, Dalton Trans. 46 (2017) 9934–9950, https://doi.org/10.1039/C7DT00644F.

[44] K.A. Tarach, K. Gołąbek, M. Choi, K. Góra-Marek, Quantitative infrared spectroscopic studies and 2D COS analysis of xylenes isomerization over hierarchical zeolites, Catal. Today 283 (2017) 158–171, https://doi.org/10.1016/J.CATTOD.2016.02.035.

[45] P. Painter, M. Starsinic, M. Coleman, Determination of functional groups in coal by Fourier transform interferometry, in: J.R. Ferraro, L.J. Basile (Eds.), Fourier Transform Infrared Spectra, Academic Press, San Diego, 1985, pp. 169–241, https://doi.org/10.1016/B978-0-12-254104-9.50011-0.

[46] D.P. Serrano, J. Aguado, J.M. Escola, J.M. Rodriguez, A. Peral, Catalytic properties in polyolefin cracking of hierarchical nanocrystalline HZSM-5 samples prepared according to different strategies, J. Catal. 276 (2010) 152–160, https://doi.org/10.1016/j.jcat.2010.09.008.

[47] K.A. Tarach, K. Pyra, S. Siles, I. Melián-Cabrera, K. Góra-Marek, Operando study reveals the superior cracking activity and stability of hierarchical ZSM-5 catalyst for the cracking of low-density polyethylene, ChemSusChem 12 (2019) 633–638, https://doi.org/10.1002/cssc.201802190.

[48] C. Lamberti, E. Groppo, G. Spoto, S. Bordiga, A. Zecchina, Infrared spectroscopy of transient surface species, Adv. Catal. 51 (2007) 1–74, https://doi.org/10.1016/S0360-0564(06)51001-6.

[49] I. Noda, Y. Ozaki, Two-Dimensional Correlation Spectroscopy: Applications in Vibrational and Optical Spectroscopy, Wiley, 2004, https://doi.org/10.1002/0470012404.

[50] N.B. Colthup, L.H. Daly, S.E. Wiberley, Chapter 3 – molecular symmetry, in: N. B. Colthup, L.H. Daly, S.E. Wiberley (Eds.), Introduction to Infrared Raman Spectroscopy, second ed., Academic Press, 1975, pp. 119–178, https://doi.org/10.1016/B978-0-12-182552-2.50006-1.

[51] E.G. Derouane, Factors affecting the deactivation of zeolites by coking, Stud. Surf. Sci. Catal. 20 (1985) 221–240, https://doi.org/10.1016/S0167-2991(09)60173-7.

[52] J.F. Haw, J.B. Nicholas, W. Song, F. Deng, Z. Wang, T. Xu, C.S. Heneghan, Roles for cyclopentenyl cations in the synthesis of hydrocarbons from methanol on zeolite catalyst HZSM-5, J. Am. Chem. Soc. 122 (2000) 4763–4775, https://doi.org/10.1021/ja994103x.

[53] K. Gołąbek, K.A. Tarach, K. Góra-Marek, 2D COS analysis of m-xylene transformation over medium-pore zeolites, Microporous Mesoporous Mater. 266 (2018) 90–101, https://doi.org/10.1016/J.MICROMESO.2018.02.028.

[54] Y. Ganjkhanlou, E. Groppo, S. Bordiga, M.A. Volkova, G. Berlier, Incorporation of Ni into HZSM-5 zeolites: effects of zeolite morphology and incorporation procedure, Microporous Mesoporous Mater. 229 (2016) 76–82, https://doi.org/10.1016/J.MICROMESO.2016.04.002.

[55] K. Pyra, K.A. Tarach, A. Śrębowata, I. Melián-Cabrera, K. Góra-Marek, Pd-modified beta zeolite for modulated hydro-cracking of low-density polyethylene into a paraffinic-rich hydrocarbon fuel, Appl. Catal. B Environ. 277 (2020), 119070, https://doi.org/10.1016/J.APCATB.2020.119070.

[56] P. Magnoux, C. Canaff, F. Machado, M. Guisnet, Coking, aging, and regeneration of zeolites XIII. Composition of the carbonaceous compounds responsible for the deactivation of a USHY zeolite during toluene disproportionation, J. Catal. 134 (1992) 286–298, https://doi.org/10.1016/0021-9517(92)90228-A.